Winter 12-1-2012

LabVIEW Based Whispering Gallery Mode Microtoroid Coupling PID Controller

Peiyao Li
Washington University in St Louis

Washington University in St. Louis
School of Engineering and Applied Science
Department of Electrical and System Engineering

Thesis Examination Committee:
Lan Yang, Chair
Paul Min
Barry Spielman

LabVIEW Based Whispering Gallery Mode Microtoroid Coupling PID Controller

by

Peiyao Li

A thesis presented to the School of Engineering
of Washington University in partial fulfillment of the
requirements for the degree of

Master of Science

December 2012
Saint Louis, Missouri

ABSTRACT OF THE THESIS

LabVIEW Based Whispering Gallery Mode Microtoroid Coupling PID Controller

by

Peiyao Li

Master of Science in Electrical Engineering

Washington University in St. Louis, 2012

Research Advisor: Professor Lan Yang

The aim of this thesis is to test the implementation of PID control algorithm for stabilization of coupling. Efficient and robust coupling is prerequisite in microcavity related applications. But surrounding environments, like temperature and airflow, could easily influence coupling condition. PID algorithm has been used for stabilization and control in industry for several decades. For this reason, the author decided to test further application, with the goal of proving the suitability for Whispering Gallery Mode coupling.

The thesis first discusses the Whispering Gallery Mode microtoroid, especially its relative coupling regime. In a second stage, the LabVIEW and Arduino based real time control system structure is introduced. And then, the PID control algorithm is discussed. Finally, experiments results are charted to prove the stability and robust coupling.

The results of experiment show that PID algorithm is well suited to stabilize the coupling system. However, due to the nonlinearity of the system, the PID coefficients need to be approximately adjusted in different coupling cases.

Acknowledgements

The research presented has been carried out at the Electrical and System Engineering Department, Washington University in Saint Louis. Working on this project is more than just learning scientific facts and obtain the conclusions. Rather, it is a training process that helps me build analytical thinking skills and triggers my desire to do research in the future.

I acknowledge my debt to those who have helped me along the way. In particular, I will to express my gratitude to my research advisors, Dr. Lan Yang, and Dr. Sahin Ozdemir for their continued encouragement, trust and invaluable suggestions during the most tough time of my study.

Furthermore I am deeply indebted to all the people at Nano Optic Lab. I would like to thank Dr. Jiangang Zhu and Mr. Bo Peng for sharing their experience and knowledge in experiment and simulation, and Fuchuan Lei, for his generous host of happy hour. Support from many others at this lab is also recognized and greatly appreciated. It is, however, not possible to list all here.

Finally I want to thank my mother. The encouragement and support from her, even in the valley of my life, once again strengthens my faith to keep moving forward. I also thank my dead father. Although I cannot share the happiness with him anymore, his words would always lead me.

Peiyao Li

Washington University in Saint Louis

December 2012

Dedicated to my parents

Contents

List of Tables

List of Figures

Chapter 1

Introduction

1.1 Thesis Outline

Recently, Whispering Gallery Mode microresonators become rapidly emerging class of optical resonators. Different from conventional optical resonator using reflect mirrors to get interference, the light is confined within the microresonators. The definition of whispering gallery modes is due Lord Rayleigh, who studied the characteristics of the so-called Whispering Gallery, namely the circular gallery, 32 meters in diameter. On the other hand, microresonator possesses many advantages over traditional optical resonators. Unlikely traditional resonator's bulky size and expensive price, the microresonator, like microtoroid, could be fabricated on silicon chip in Nano scale with extremely low expense.

In the last decade, researchers have presented many useful and promising applications based on microresonators. The Nano/micro-mechanical sensors detect particles by monitoring the resonance frequency changes caused by the additional effective mass of the binding particles, while resonator-based micro/Nano-optical resonator sensors rely on the resonance frequency shift due to the change in the effective polarizability of the resonator-environment system upon particle binding. Scientists have also invented the single particle level sensor based on Ultra-high-Q microtoroid. In sum,

micro resonator has shown its ability and potential for the bio sensing and other kind of sensor related applications.

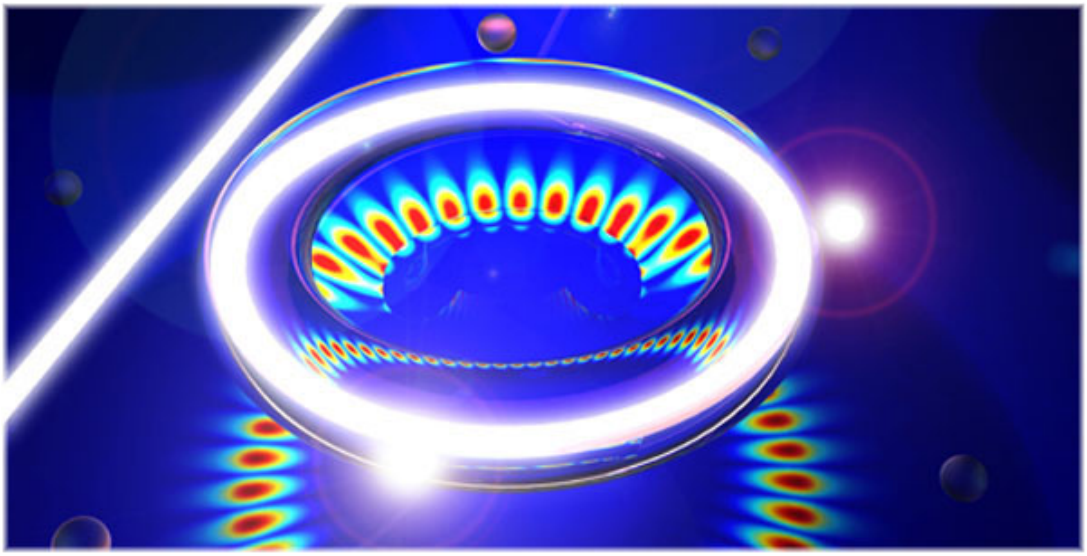

Figure1.1 A Simulated Image of the On-chip Microtoroid-taper Coupling System

However, for the microresonator, due to its superior sensitivity of to the changes in surrounding environment, like air flow, humidity or temperature, the coupling condition between taper and microresonator would be easily changed, which results in the fluctuation of signal. The result of some experiments about using WGM resonators for sensing would be deteriorated. This is the case we try to get rid of.

PID algorithm is a mature industrial control algorithm for stabilization using feedback. Many areas utilize PID for control, ranging from basic temperature control to auto cruise function on vehicles. In this thesis, we utilize the PID algorithm to stabilize the air gap distance.

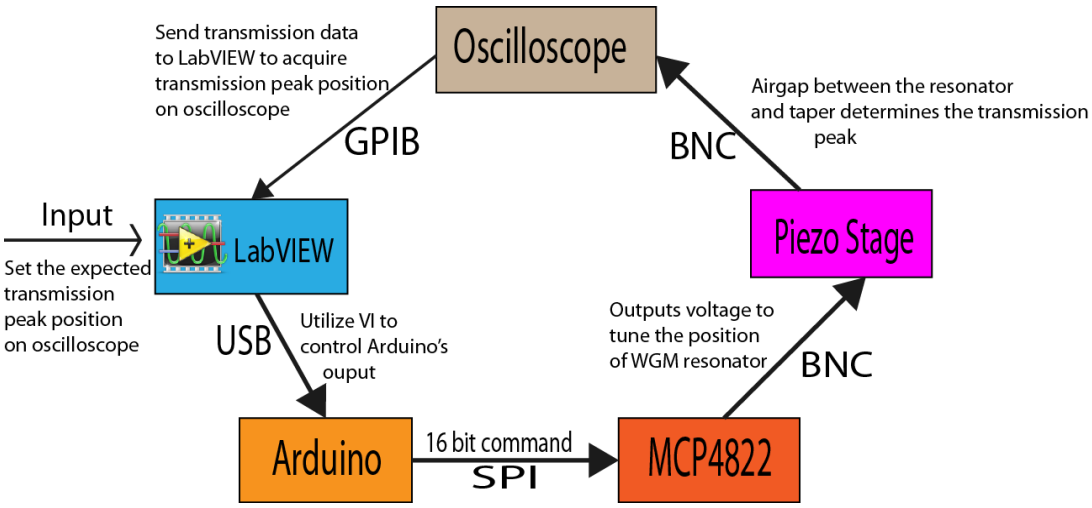

Figure1.2 LabVIEW Based PID Controller System Structure

In our lab, people using LabVIEW to acquire data from oscilloscopes. And LabVIEW has shown researchers its superior ability to support the scientific research. So we combined LabVIEW application development with PID control. Using the MCP4822, a 12-bit DAC chip, we obtain the precise control to the Piezo stage.

Figure1.1 is the LabVIEW based PID controller system structure. The results of experiments demonstrate that the control scheme with PID and LabVIEW is practical and reliable. Compared with case when there is no PID controller, our system could stable the coupling under air flow and thermal noise. However, due to nonlinearity of coupling system, we cannot get an ideal PID algorithm.

1.2 Chapter Overview

Chapter 2 is an introduction to WGM microresonator and its coupling to taper. Different aspects of the microresonator, such as their geometry, quality factor and

coupling methods are introduced. The main device for this thesis is microtoroid. Since this thesis focus on the stabilization and control of coupling, the coupling theory would be studied in this chapter.

Chapter 3 introduces LabVIEW and Arduino platform. The history and advantages of LabVIEW software would be introduced. We would also talk about the architecture of PID control application. Detailed design of application is presented. In the second section of this chapter, Arduino UNO board and related connection would be presented in detail.

Chapter 4 solves problem on conversion between digital signal analog signals and gives the solution for precise analog voltage output control using LabVIEW. The principle of PWM and how to get DC voltage is studied here. The main topic in this chapter is about using SPI bus for output voltage. The principle and advantages would be studied. Specific circuits using MCP8422 and related LabVIEW library would also be given out in this chapter.

Chapter 5 focuses on the PID algorithm design. Since coupling system in the thesis is too complicated to analyze using system transfer function, a simple damper problem model is utilized to discuss the effects of PID coefficients. And we would also give out the manual tuning method we use in the experiment.

Chapter 6 presents the experiment result. We will analyze the results to demonstrate that our system could stabilize the coupling and control the tuning process. The limitation of system would also be discussed.

Chapter 2

Coupling of Whispering Gallery Mode Microtoroid

2.1 Introduction to WGM Microresonator

Traditional optical resonators consisting of two or mirrors are utilized in different research areas of modern optics. Critical properties of optical resonators, such as finesse and high quality factor can be achieved when high reflectivity and low loss mirrors as well as other most transparent optical elements are used.

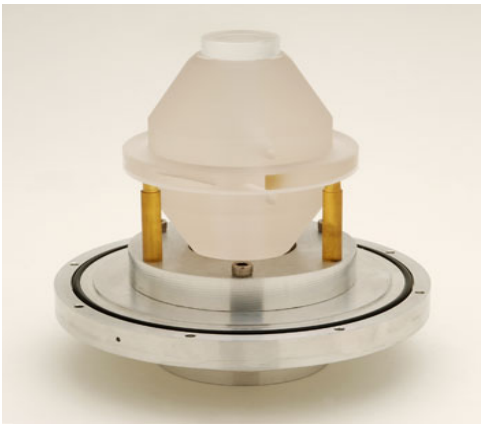

Figure2.1 ATFilms 6030 Fabry Perot Cavity from Stable Laser System

Despite conventional Fabry–Perot (FP) resonators are versatile, they have remained fairly complex and expensive, bulky, difficult to assemble, and prone to vibration

instabilities.

In the last decade, Whispering gallery mode (WGM) optical microresonators with ultra-high quality factors are of interest for a variety of scientific disciplines ranging from fundamental research to applied physics applications. Unlike the traditional optical resonator, WGM microresonator could be extremely small in size, which is in Nano scale, and very cheap as well.

The history of WGM could be tracked back almost one century ago by work of Lord Rayleigh, who studied the propagation of sound wave over a curved surface of St. Paul Cathedral. He discovered that a whisper standing against its wall at any point was audible to a listener with an ear held to the wall at any other point around the gallery. He also suggested that such propagation modes would exist for electromagnetic waves as well, and could find practical applications due to the extreme confinement of the field.

Figure 2.2 St. Paul Cathedral Whispering Gallery

Similarly, ray of light could propagate along the spherical boundary of microcavity by internal reflection and be confined in the cavity as shown in Figure 2.3:

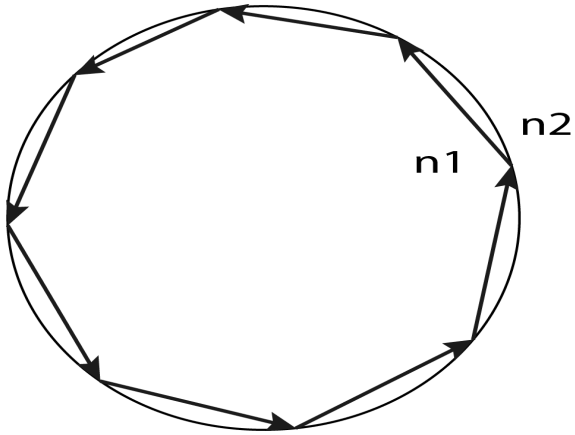

Figure2.3 Propagation of Light Ray in a Spherical Cavity

There are many types of WGM microresonators, divided by their geometry shapes. (Figure 2.4)

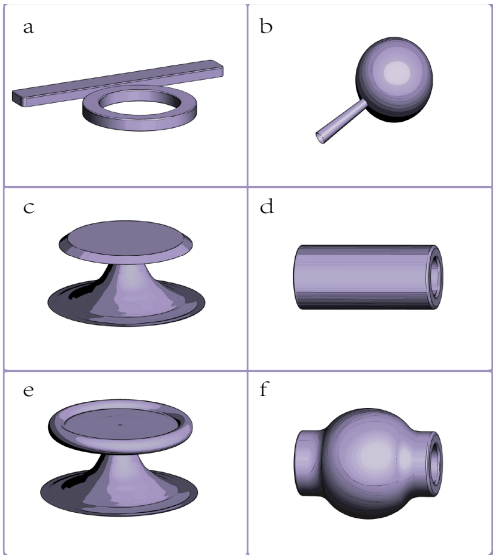

Figure2.4 Different Types of Microresonators

For example, the most popular microresonator is probably microspheres (2.4.b). They

can be easily fabricated by melting the tip of a taper fiber. A silica sphere is formed naturally by surface tension of the melted glass material. Micro-cylinder (2.4.d) and micro-bottle (2.4.f) can be fabricated by heating and pulling glass tubes while inflates the softened material with inert gas. Microring (2.4.a), microdisk (2.4.c) and microtoroid (2.4.e) are fabricated on silicon chip by standard micro fabrication techniques, thus can be mass-produced.

In this thesis, the microresonator we refer is microtoroid:

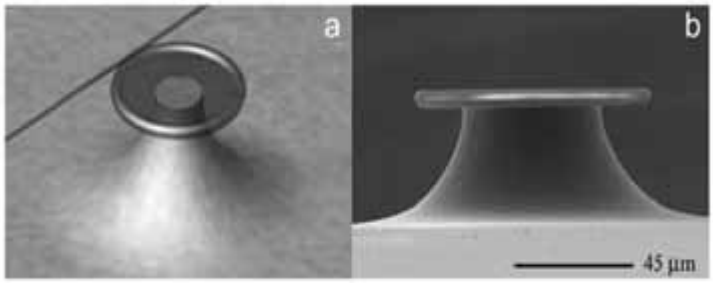

Figure2.5 the Ultra-high-Q (UHQ) Microtoroid Resonator: a) A rendering of the UHQ microtoroid coupled to a tapered optical fiber waveguide and b) SEM of the UHQ microtoroid resonator.

For the microresonators, the most important parameter of merit is its quality factor, or Q factor. It quantifies the resonator's optical quality and describes its ability to confine light. The Q factor is defined as the ratio of energy stored in the resonator to the amount of dissipated energy per optical cycle:

$$Q = 2\pi \frac{E_{stored}}{E_{dissipated}} \qquad (2.1)$$

2.2 Coupling Scheme and Theory

Efficient controllable coupling, that is, proper air gap, is the critical and prerequisite requirement of feasibility of practical applications of the resonators, can only be achieved via the near field of a WGM.

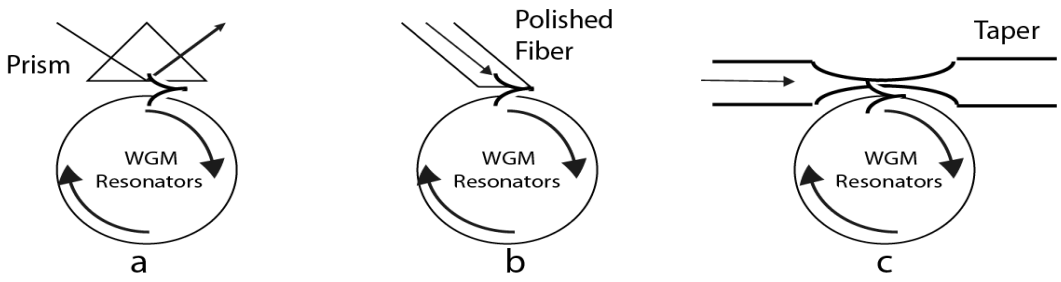

Figure2.6 Different Coupling Schemes: a. Prism b. Polished Fiber c. Taper

In the laboratory, we choose to couple the microtoroid with a fiber:

> Tapered optical fibers allow both efficient excitation and extraction of optical power from the same fiber, while maintaining fiber-optic compatibility. Using tapered optical fibers we have achieved very efficient excitation of whispering gallery modes and observed the condition of 'critical coupling'. Of even greater significance is that the fiber taper junction is highly "ideal" meaning that its behavior closely approximates a perfect two-mode coupler… [1]

Tapered optical fibers are easily made by heating a single-mode fiber with a torch and slowly pulling the fiber apart until a waist region only a few microns in diameter is created.

To analyze the relationship between air gap and on resonance transmission T_{ON}, we have the Figure 2.7 below to illustrate different coupling mechanisms within a taper-microtoroid system.

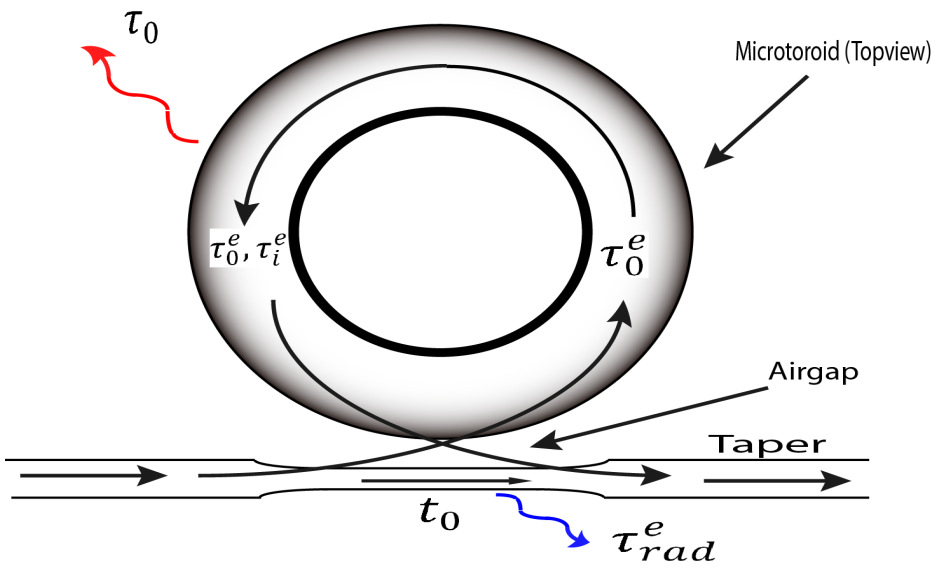

Figure 2.7 Different Coupling Mechanisms Within a Taper-microtoroid System

We assume that conditions are that internal resonator loss is small and coupling is week. If so, the contributions of waveguide-induced cavity loss and intrinsic cavity loss are separable. Therefore,we could get the internal cavity field ('E') by taking all sources of caivity loss:

$$\frac{dE}{dt} = i\Delta\omega E - \frac{1}{2}\left(\frac{1}{\tau_0} + \frac{1}{\tau_{rad}^e} + \sum_{i=0}\frac{1}{\tau_i^e}\right)E + i\sqrt{\frac{1}{\tau_0^e}}E \qquad (2.2)$$

Here τ_0 is the intrinsic resonator photon lifetime, τ_{rad}^e is the lifetime for coupling/scattering to radiation modes, and τ_i^e denotes the coupling lifetime for coupling to each supported waveguide mode (τ_0^e represents the fundamental waveguide mode which is always present). The last term gives the excitation of the

cavity due to only the fundamental waveguide mode with amplitude denoted by s under adiabatic tapering conditions.

We could have on resonance transmission T_{ON} as below equation:

$$T_{ON} = T_{CC} + (1 - T_{CC})(\frac{1-K}{1+K})^2 \quad (2.3)$$

where T_{CC} is the finite on resonance transmission at critical coupling induced by the polarization ellipticity in the loop and K denotes a dimensionless coupling parameter. To make calculation an anlysis simpler, we set K as:

$$K = \frac{\gamma_e}{\gamma_i} \quad (2.4)$$

γ_e is the extrinsic coupling rate and $\gamma_i = (2\pi/\lambda_0)/Q_{in}$ is the intrinsic cavity loss rate, λ_0 is the center wavelength of resonance and Q_{in} is the intrinsic Q factor. We expect γ_e changes exponentially with the air gap d, that is:

$$\gamma_e = \gamma(0)\exp(-\eta d) \quad (2.5)$$

Where $\gamma(0)$ is the extrinsic coupling rate at zero distance, and η is the decay constant, we suppose it to be $\eta = \frac{1}{404} nm^{-1}$.

- When K = 1, $T_{ON} = T_{cc}$, we have critical coupling: the coupling is strong while the total quality is not degradateddegraded so much

- When K > 1, we have over coupled: the microtoroid is quite close to the taper, the coupling is so strong that the coupling loss reflected on the output transmission is pretty obvious.
- When K < 1, we have under coupling: microresonator is far from the tapered waveguide, the coupling is weak

After simulation, we got the Figure2.7 below:

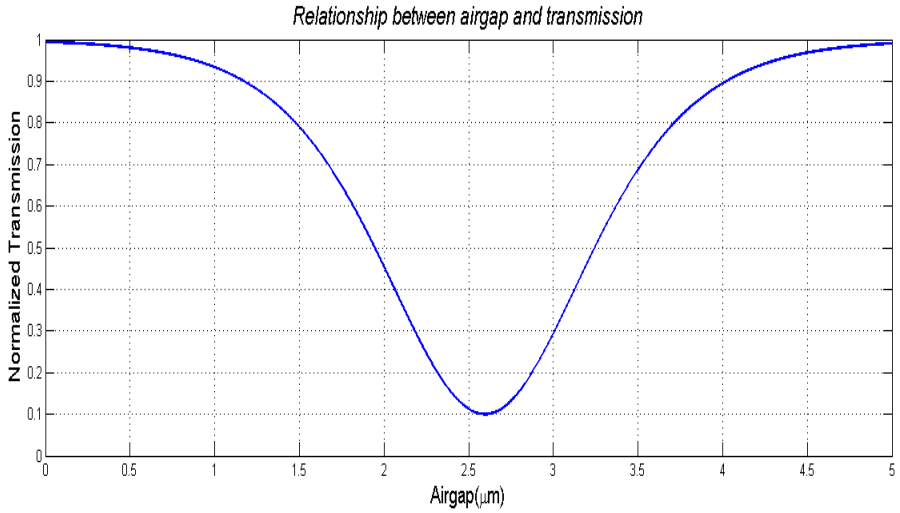

Figure 2.8 Simulation Results of Transmission According to Different air gap

Figure 2.8 is the real measurement picture get by researchers, whose fitting curve is similar with our simulation results

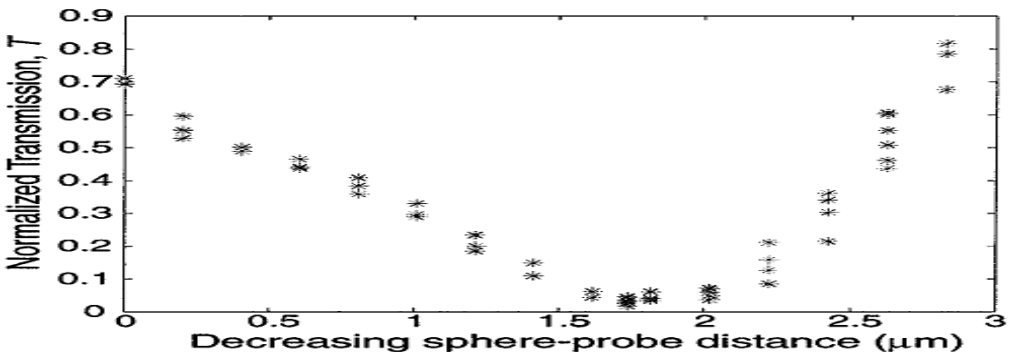

Figure 2.9 Normalized Transmissions as a Function of The Probe Position [2]

From the simulation results, we could find that the relationship curve between air gap and on resonance transmission is a Lorenz curve. However, in a specific range of air gap, for instance, 1.5um- 2.5um, on resonance transmission is approximately linear with air gap. This conclusion gives us clue that we could control and stabilize the coupling by tuning air gap.

2.3 Experiments Setup

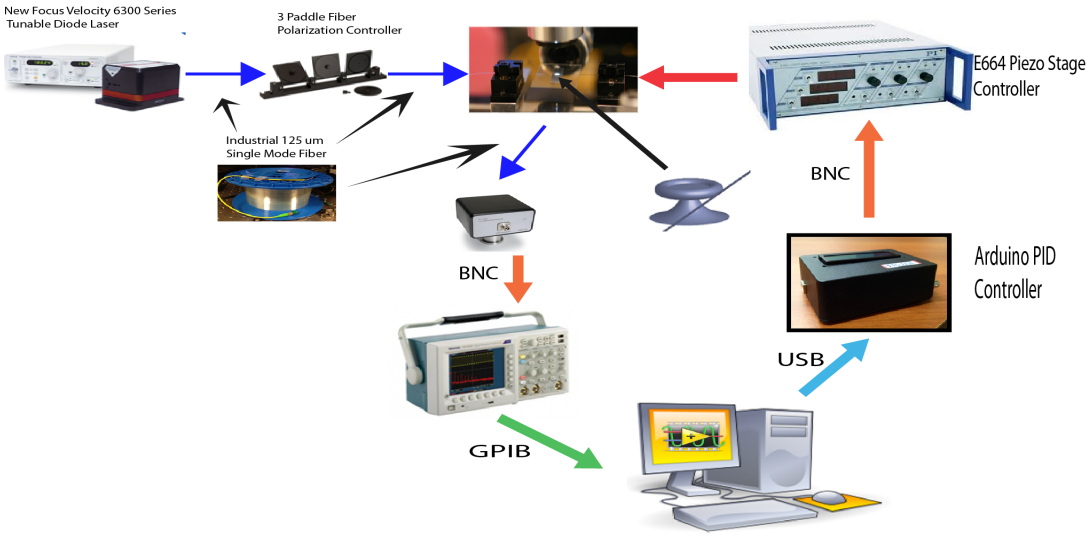

Figure 2.10 Experiment Setup

Figure 2.10 display our experiment set up. In our experiments, we use devices below:

- Laser Source: New Focus Velocity 6300 Series Tunable Diode Laser (as reference).
- Polarization Controller: 3 Paddle Fiber Polarization Controller.
- Fiber Waveguide with a Tapered Area: Industrial 125 um Single Mode Fiber (the tapered area on the pulling stage is about 20mm in length and 1-2um in thickness).
- Photo detector: New Focus 1811 Low Noise Photo detector (as reference).

- On-Chip Micro-Cavity : On-chip Microtoroid, Microdisk, or Microsphere.
- Three-Dimensional External Nano-Positioning Stage: PI 3-D Piezo Nano-Positioner & Servo Controller (as reference).
- Arduino Based PID controller: PID Coup Controller.
- High Speed Oscilloscope: Tektronix TDS3014B Digital Oscilloscope (as reference).

Chapter 3

LabVIEW and Arduino Platform

In this chapter, the LabVIEW (Laboratory Virtual Instrument Engineering Workbench) and Arduino based real time control system structure is introduced. In the thesis, we use LabVIEW to conduct data acquisition, PID algorithm control and writing binary code command to Arduino UNO board through LabVIEW Interface for Arduino (LIFA). On the Arduino side, 16 bit binary code is written to MCP4822 12-bit DAC through SPI, which outputs control voltage to Piezo stage. The advantages of LabVIEW and Arduino would also be discussed and analyzed.

3.1 LabVIEW Develop Environment

LabVIEW is a graphical programming environment based on graphical programming language G. Execution of program is determined by the structure of a graphical block diagram. Programmer connects different function-nodes by drawing wires. These wires propagate variables and any node can execute as soon as all its input data become available. Since this might be the case for multiple nodes simultaneously, G is inherently capable of parallel computation. Multi-processing and multi-threading hardware is automatically exploited by the built-in scheduler, which multiplexes multiple OS threads over the nodes ready for executions.

3.1.1 LabVIEW History and Advantages

The beginning of LabVIEW could be date back to the 1980s when Macintosh Company produced first computer using graphical user interface. Graphical user interface enable flow chart on computer screen. And this inspired Jeff Kodosky, "father of LabVIEW" for graphical programming. Since he was mostly using data acquisition in his work area, he started to create a novel graphical programming language based on flow chart rather than traditional sequential processing. In 1986 the first version of LabVIEW, LabVIEW 1.0, was published (Figure 3.1), which was similar as we see today. The main goal of this programming at that time was to simplify data acquisition from GPIB bus. And we still rely on this feature in our research nowadays.

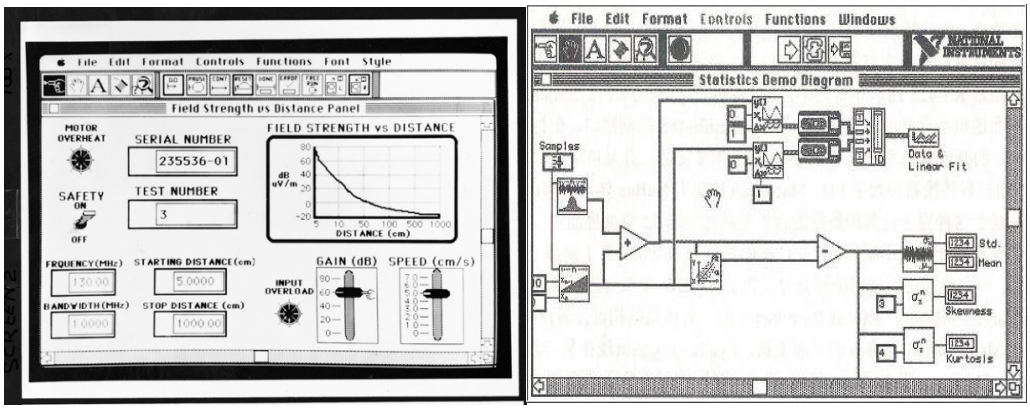

Figure3.1 the Block Panel and Front Panel of LabVIEW 1.0

3.1.2 LabVIEW Based Application

The Basic structure of application is displayed as below (Figure 3.2):

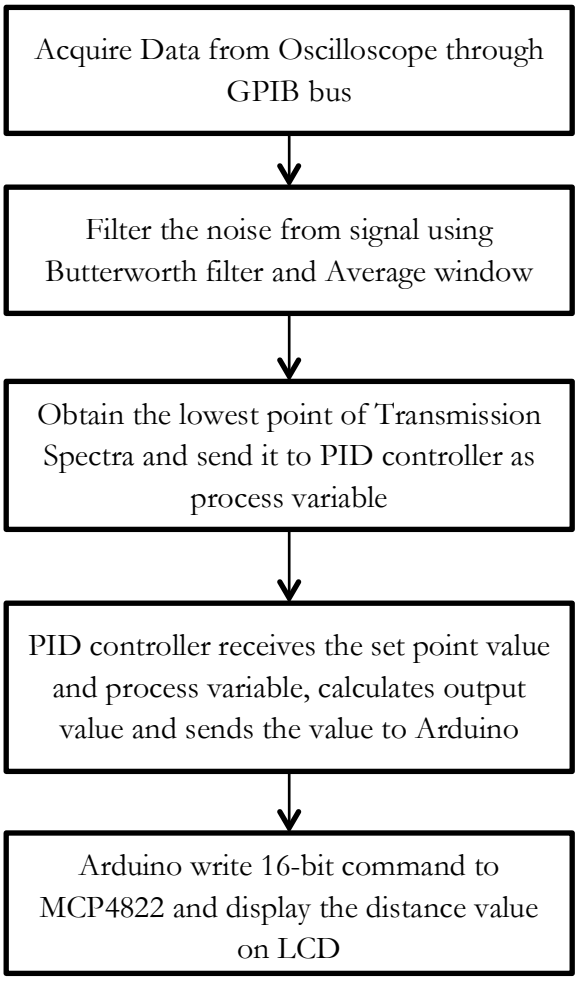

Figure 3.2 LabVIEW Based Application Architecture.

In the first stage, LabVIEW program communicates with Tektronix TDS oscilloscope through the GPIB bus and obtain the waveform of resonance displayed on oscilloscope. This part is shown in Figure 3.3.

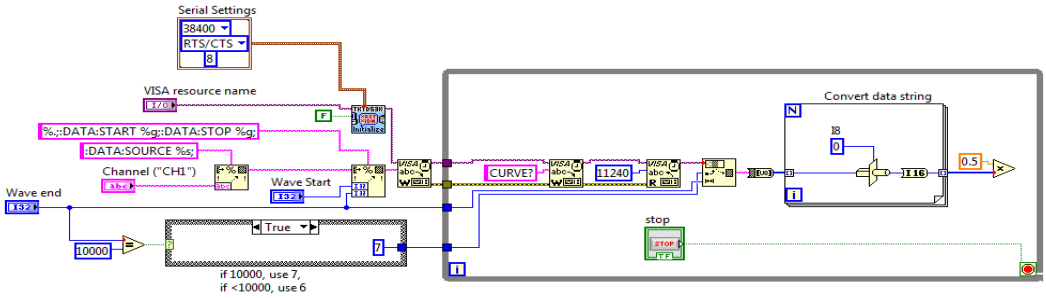

Figure 3.3 Data Acquisition in LabVIEW Through GPIB

In the second stage, we process the raw signal from oscilloscope, which has much noise. We average the signal first to get the precise baseline. And then we filter the signal with 5th order Butterworth filter band pass filter. After we get the filtered signal, we use the "Array Min& MAX" VI in LabVIEW to obtain the lowest point of the valley. (Figure 3.4)

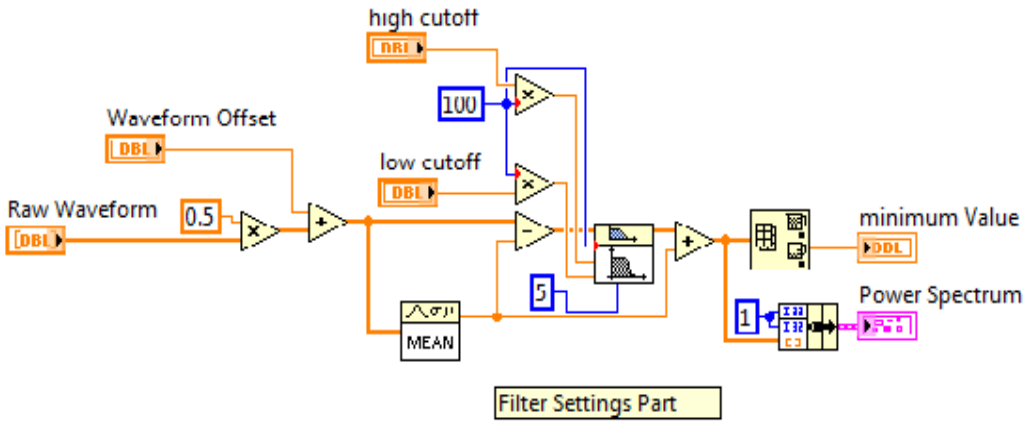

Figure 3.4 How to Filter the Noise from Raw Signal

The core part is using PID control module in LabVIEW to conduct the air gap control and coupling stabilization. This part is shown in figure 3.5. The input of PID controller VI is setpoint, process variable, output range, PID gains, and dt. Setpoint specifies desired value of the process variable being controlled. In our case, this variable controls the desired position of lowest point on Oscilloscope. Process variable is the measured value in system, which should be the lowest point's position achieved from last stage. PID gains are the PID algorithm's parameters, which would be discussed in Chapter 5. The two orange arrows in the block are called shift register, which stores the output value from the last loop and delivers it to the next loop.

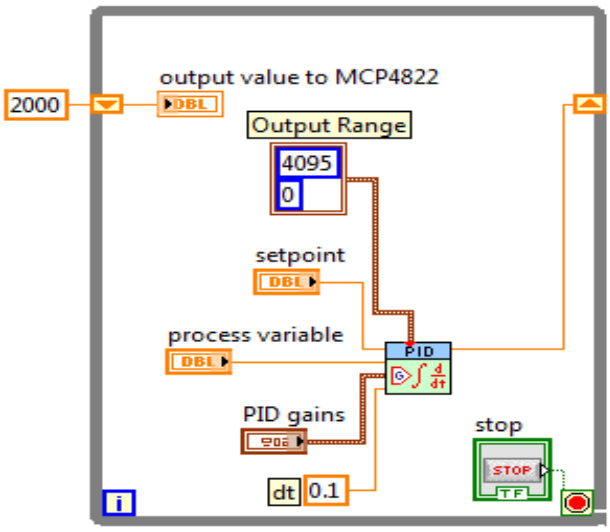

Figure 3.5 PID Control Module in LabVIEW

The Final stage is the collaboration between LabVIEW and Arduino. We get the output value in decimal from PID controller and input that value in binary to the Arduino. Arduino wraps this value with other command in binary code and passes it to MCP4822 through SPI protocol. In our product, we also utilize a 16*2 LCD to display the moving average and indicate the stable status. (Figure 3.6)

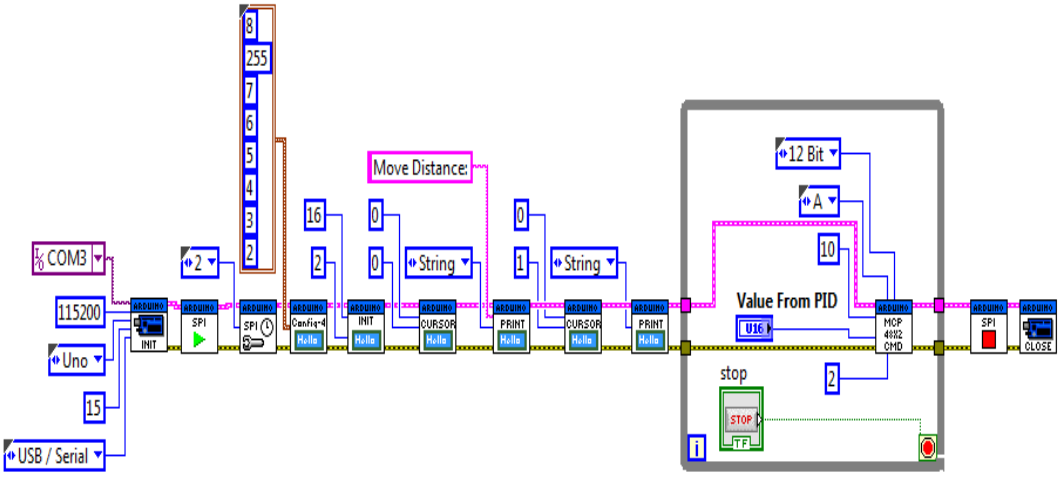

Figure 3.6 Arduino Control and LCD Display Block

Figure 3.7 is the front panel of application. We set the PID controller parameters here. Figure 3.8 is the real time PID control window. Yellow line is the measurement

transmission's peak positions. Red line is the set point.

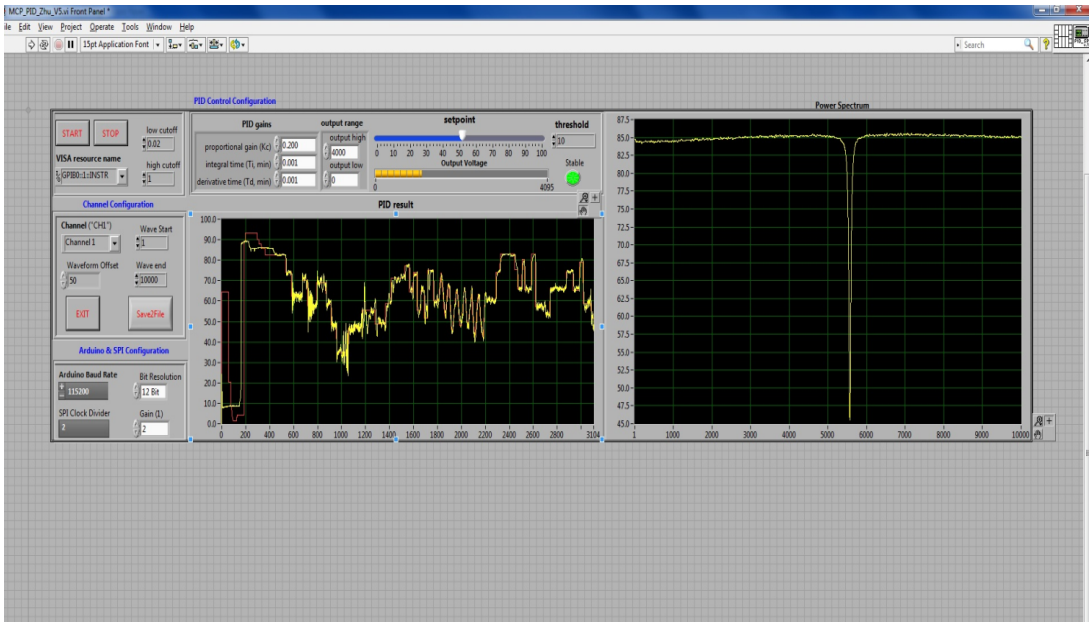

Figure 3.7 Application front panel

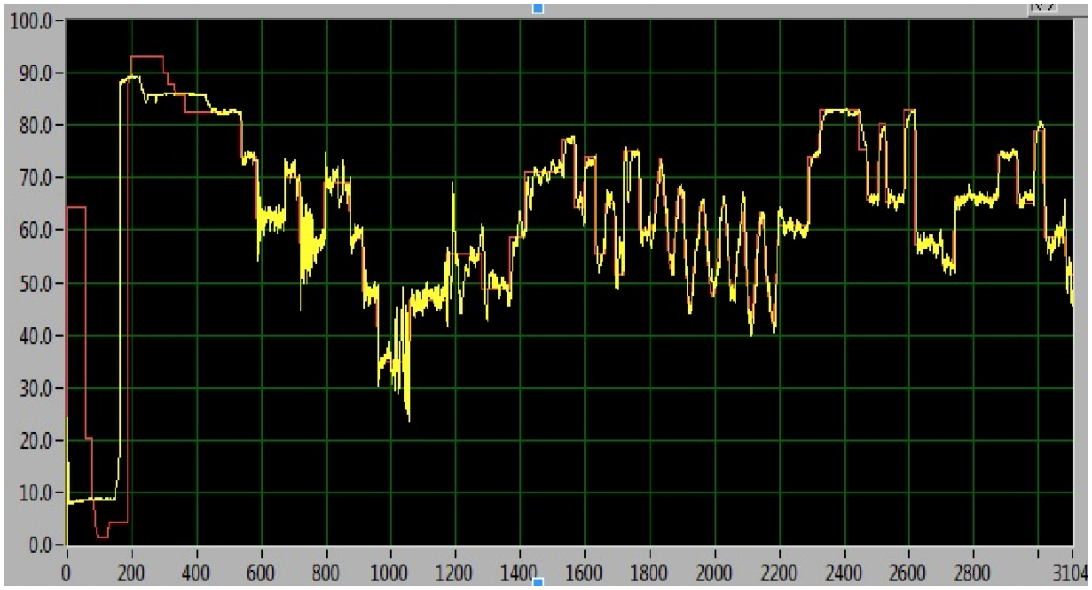

Figure3.8 PID Controller Result Window

3.2 Arduino UNO Board

Arduino is an open-source physical computing platform based on a simple microcontroller board, and a development for writing software for board.

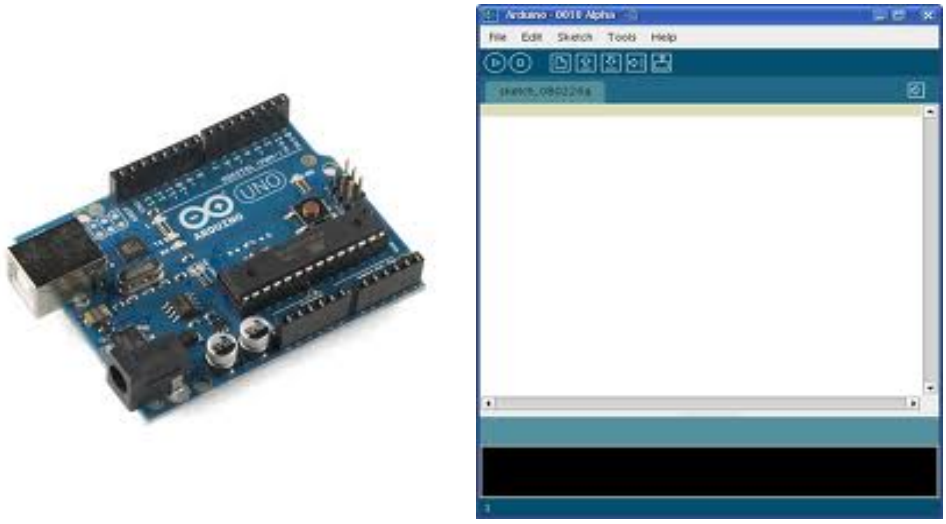

Figure3.9 Arduino Hardware and Software: a) Arduino UNO board b) Arduino IDE

There are many other microcontroller platforms available for the physical computing, like Phidgets, MIT's handyboard with similar functionality. All of these boards wrap up the messy details of microcontroller programming to easy-to-use package. However, Arduino possesses its own advantages over other platforms.

- Cross-platform: The Arduino software runs on Windows, MacOS and Linux while most other microcontroller could only run on Windows.
- Simple and clean programming environment: Arduino is easy-to-use for beginners, but flexible and powerful enough for experienced users.
- Open-source and extensive software/ Hardware: The Arduino software is published as open source tools, available for extension by experienced programmers. The language can be expanded through C++ libraries. The

Arduino is based on Atmel's ATMEGA8 microcontroller. The plan for module is published under a Creative Common Licenses. So advanced users could extend it to more functional version.

- Inexpensive: The general price of Arduino UNO is around only $20, which is very cheap
- LabVIEW interface: National Instruments develops the LabVIEW interface for Arduino. This interface enables us to make full use of LabVIEW powerful VI library to work with Arduino for research.

Table3.1 below list the hardware configuration of Arduino:

Table3.1 Arduino Configuration Summary

Hardware	Detail
Microcontroller	ATmega328
Digital I/O Pins	14(of which pin
Analog Input Pins	6
Flash Memory	32KB
SRAM	2KB
EEPROM	1KB
Clock Speed	16MHz

Chapter 4

Analog Output Schemes

In the last chapter, we talked about the system structure and application architecture in LabVIEW. In this chapter, we will discuss two analog output schemes: Pulse Width Modulation (PWM) with RC low pass filter and 12-bit DAC Chip MCP using Serial Peripheral Interface (SPI). Arduino Uno has the digital PWM output with pin, and SPI output with pin as well.

4.1 Pulse Width Modulation

4.1.1 Introduction

Pulse Width Modulation (PWM) is a powerful technique to control analog output circuit with a processor's digital signals. PWM is employed in a wide variety of applications, ranging from power control to measurement and communications system.

Pulse Width Modulation uses a rectangular pulse wave whose pulse width is modulated resulting in the variation of the average value of the waveform. If we consider a pulse waveform with a highest value V_{max}, a lowest value V_{min}, and a duty cycle D, the average value of the waveform is given by:

$$\bar{V} = \frac{1}{T}\int_0^T f(t)dt \qquad (4.1)$$

As $f(t)$ is a pulse wave, its value is V_{max} for $0 < t < DT$, and V_{min} for $DT < 0 < T$, equation 3.1 could be expressed as:

$$\bar{V} = \frac{1}{T}\left(\int_0^{DT} V_{max}dt + \int_{DT}^{T} V_{min}dt\right)$$

$$= \frac{D * T * V_{max} + (1 - D) * T * V_{min}}{T}$$

$$= D * V_{max} + (1 - D) * V_{min} \qquad (4.2)$$

In our case, V_{max} is 5V and V_{min} is 0V, therefore we obtain:

$$V = D * 5 \quad (4.3)$$

This means we could control output voltage by time duty cycle.

For the Arduino, we write a value from 0 to 255 to a PWM pin, and the Arduino library will cause the pin to output a PWM signal whose on time is in proportion to the value written.

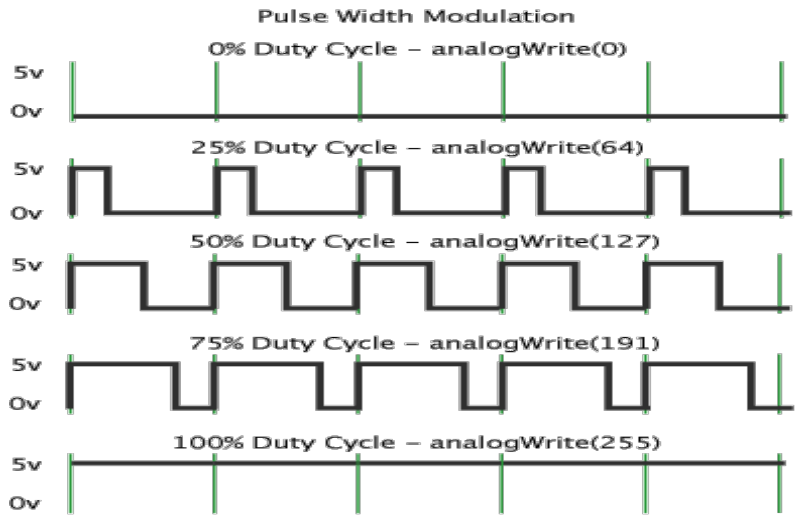

Figure 4.1 PWM Signal with Different Time Duty Cycles

The Arduino has its own set default values. For pins 3, 9, 10, and 11，PWM frequency is approximately 488 Hz. For pins 5 and 6, it is about 977 Hz. These values are for a Arduino running at 16MHz. We can change these frequencies easily by writing new values to the appropriate timer register. For example, to change the frequency of timer 2, which controls pins 9 and 10, to 3,906 Hz, you would set its register like so:

```
TCCR1B = TCCR1B & 0b11111000 | 0x02;
```

4.1.2 RC Low Pass filter Analysis

To get analog signal, we have to pass the PWM signal through low pass filter circuit as below.

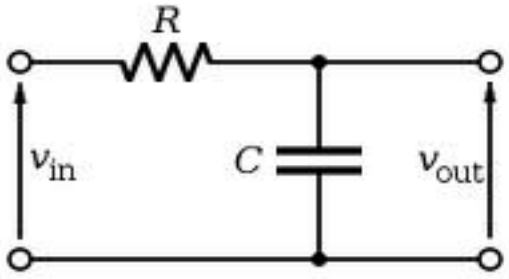

Figure 4.2 RC Low Pass Filter Circuit

If we examine the circuit on the left, when an input voltage is applied to the input of R, the capacitor C will begin to charge. When it is charged, it will stop to conduct current and the voltage at the output will match the input. Capacitors block DC currents but pass AC currents. We can see that any DC voltage input would be output, but high frequency AC voltages will be shorted to ground. The cutoff frequency is determined by time constant:

$$f_c = \frac{1}{2\pi RC} \qquad (4.4)$$

Although this is a very simple circuit, there is tradeoff while choosing the appropriate values for resistor and capacitor – that is, how much ripple can we tolerate and how fast does the filter need to respond? In most filters, we would like to have the perfect filter – one that passes all frequencies below the cutoff frequency, with no voltage ripple. While no such ideal filter exists, we can achieve close to it by using a multiple pole filter. Such a filter would incorporate many components in a ladder configuration. Even though such a filter has wonderful performance characteristics, its complexity and cost is unnecessary for simple D-A conversion.

4.2 Serial Peripheral Interface

In this section, we will discuss how to output control signal with MCP4822 a 12-bit DAC chip using SPI bus. Nowadays, more and more serial bus systems are preferred instead of a parallel bus, because of the simpler wiring scheme. As the efficiency of serial buses increases, the speed advantage of the parallel data transmission gets less important. The clock frequencies of SPI devices can go up to some Megahertz and more. There are a lot of applications where a serial transmission is perfectly sufficient.

4.2.1 Introduction to SPI

Serial Peripheral Interface (SPI) is a synchronous serial data link standard, which is named by Motorola, working in full duplex mode. SPI is used primarily for a host processor and multiple peripherals, which is called master/slave mode.

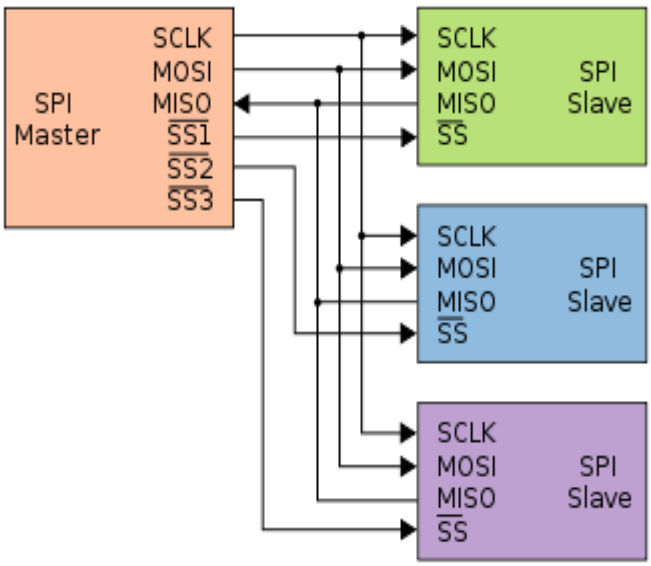

Figure 4.3 SPI Master/Slave Scheme

4.2.2 MCP4822 and Corresponding Library in LabVIEW

MCP4822 is a low power, high accuracy and low noise 12-bit Digital to Analog Converts (DACs), with optional 2x-buffered output and Serial Peripheral Interface (SPI), designed by Microchip Technology Inc.

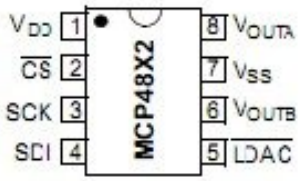

Figure4.4 Top View of MCP4822

The Function of 8 pins of MCP is shown as table below:

Table4.1 MCP4822 8-Pin Configuration

Pin Number	Symbol	Function
1	V_{DD}	Positive Power Supply Input
2	$\overline{CS}$	Chip Select Input
3	SCK	Serial Clock Input
4	SDI	Serial Data Input
5	$\overline{LDAC}$	Synchronization input
6	V_{OUTB}	DAC_B output
7	AV_{ss}	Analog ground
8	V_{OUTA}	DAC_A output

The ideal output voltage is given by equation (4.5):

$$V_{OUT} = \frac{2.048V*G*D_N}{2^n} \quad (4.5)$$

where G is the output gain, D_N represents the digital input value, and n represents the number of bits of resolution (n=12).

All write commands to MCP4822 are 16-bit words. Any clock over 16 will be ignored. The most significant four bits are configuration bits and remaining 12 bits are data bits. Illustration is shown in table below:

Table4.2 MCP4822 16-bit Command

Bit Number	**Function**
Bit 15	DAC_A or DAC_B select bit. 1 = write to DAC_A, 0 = write to DAC_B
Bit 14	Don't care
Bit 13	Output gain select bit 1 = 1x, 0 = 2x
Bit 12	Don't care
Bit 11- Bit 0	DAC data bits, containing value 0-4095

And the write command process is in figure4.4 :

Commands are sent to the device via the SDI pin, with data being clocked-in on the rising edge of SCK. The communications are unidirectional. Therefore, data cannot be read out of MCP4822. The $\overline{CS}$ must be held low for the duration of a write command

.

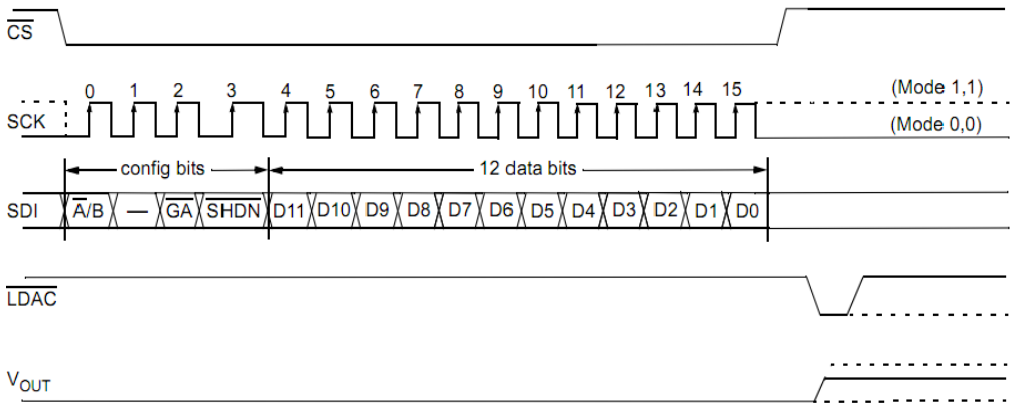

Figure4.5 Writing Command Process of MCP4822

We created corresponding LabVIEW VI library of MCP4822 so that it could communicate with Arduino in LabVIEW.

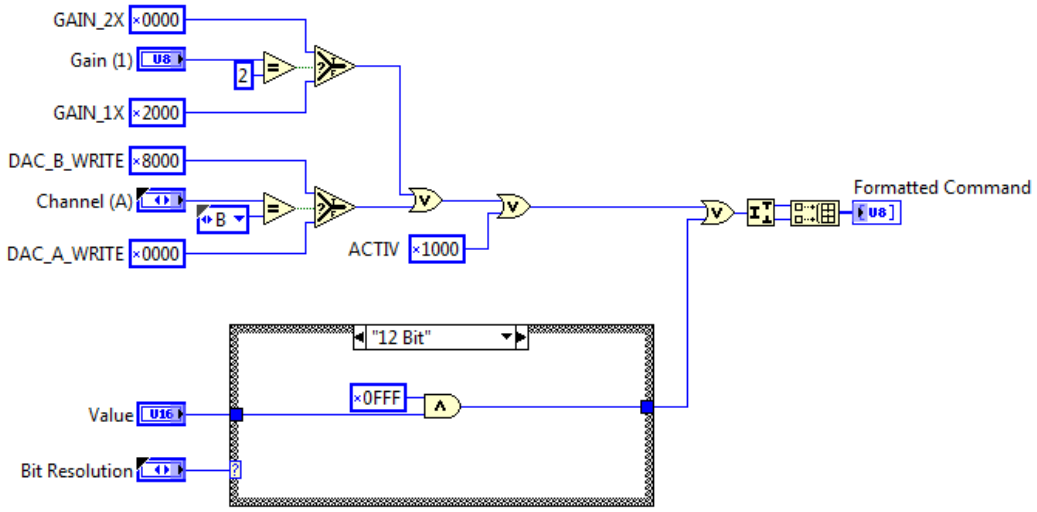

Figure4.6 Format 16-bit command in LabVIEW

Figure is the first stage to get the formatted 16-bit command written to the MCP4822.

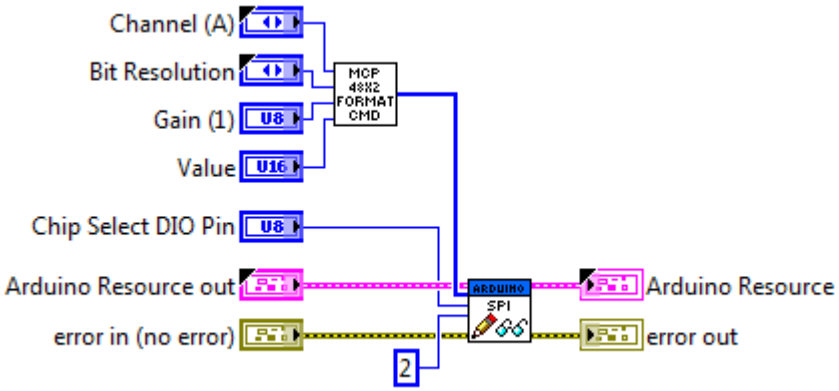

Figure 4.6 Send formatted SPI command from LabVIEW to Arduino

Figure4.6 above illustrates how to write the formatted command to Arduino using SPI write VI in LabVIEW

We connect MCP4822 with Arduino as below Figure:

CS pin with pin 10, SCK pin with pin 12, SDI pin with 13, LDAC pin with pin 9,

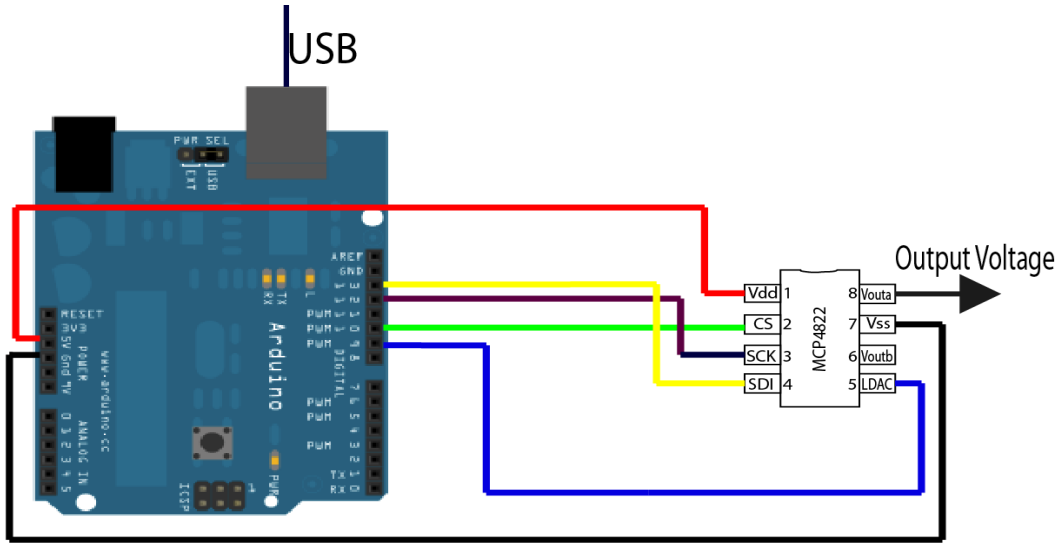

Figure4.7 Connection between Arduino and MCP4822

Chapter 5

PID Algorithm

5.1 Introduction

The PID control scheme is named after its three correcting terms, whose sum constitutes the manipulated variable (MV). The proportional, integral, and derivative terms are summed to calculate the output of the PID controller. Defining as the controller output, the final form of the PID algorithm is:

$$u(t) = K_p e(t) + K_i \int e(t)dt + K_d \frac{de(t)}{dt} \quad (5.1)$$

PID controller works in a closed-look system shown above. The variable $e(t)$ represents the error signal, which is the difference between Set Point (SP) and Process Variable (PV). This error signal will be sent back to the PID controller, and the controller computes both the derivative and integral of this error signal. The output control signal equals the sum of proportional gain (K_p) times the magnitude of error signal, integral gain times the integral of error, and derivative gain times the derivative of error signal.

This control signal is sent back to the plant, and new output is achieved. The new output then is fed back and compared with reference value to obtain the new error

signal. The controller repeats the algorithm again, ad infinitum.

The diagram (Figure 5.1) illustrates above process:

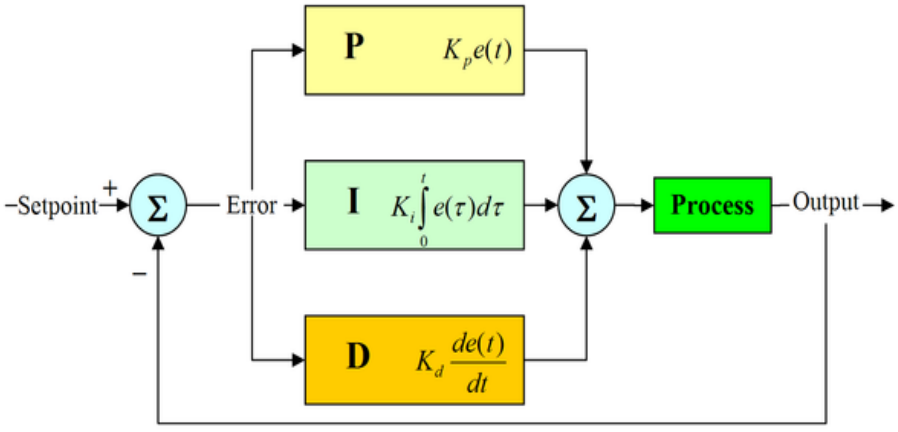

Figure 5.1 Diagram of PID Algorithm

The transfer function of a PID controller is found by taking the Laplace transform of Equation 5.1:

$$u(s) = K_p + \frac{K_i}{s} + K_d s \quad (5.2)$$

5.2 PID Coefficients

The coefficients $K_p, K_i\, K_d$ play a critical role in the PID algorithms. Our coupling is so complicated that we cannot get the accurate parameters to analyze the effects of PID coefficients. We introduce a simple system to discuss how PID parameters contribute to the system, Figure 5.2

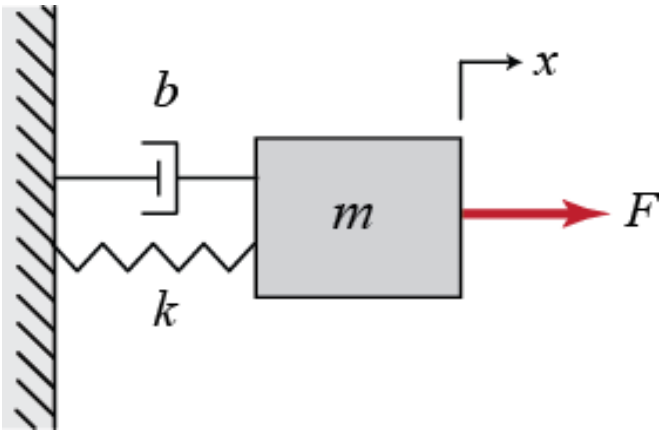

Figure 5.2 Spring-Damper Problem Model

Modeling equation of this system is:

$$M\ddot{x} + b\dot{x} + kx = F \quad (5.3)$$

Taking the Laplace transform of the modeling equation, we obtain:

$$Ms^2X(s) + bsX(s) + kX(s) = F(s) \quad (5.4)$$

Then, the transfer function between displacement $X(s)$ and input $F(s)$ becomes:

$$\frac{X(s)}{F(s)} = \frac{1}{Ms^2+bs+k} \quad (5.5)$$

Set M = 1kg, b = 15N s/m, k = 20N/m, F = 1N, we have the specific transfer function:

$$T(s) = \frac{1}{s^2+15s+20} \quad (5.6)$$

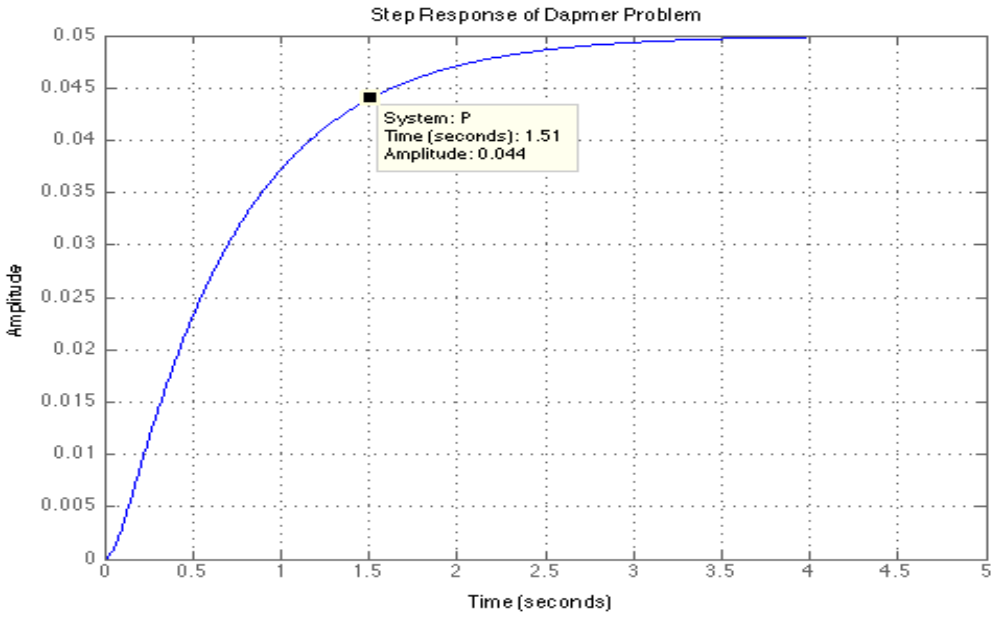

Figure 5.3 Step Response of Spring- Damper Problem

DC gain of transfer function is 1/20, so the final stable value of the output is about 0.05. The above chart also shows that the rise time of system is about 2s and steady state error is 0.95. When we introduce the P control, original transfer function becomes:

$$T(s) = \frac{K_p}{s^2+15s+(20+K_p)} \qquad (5.7)$$

Corresponding step response is:

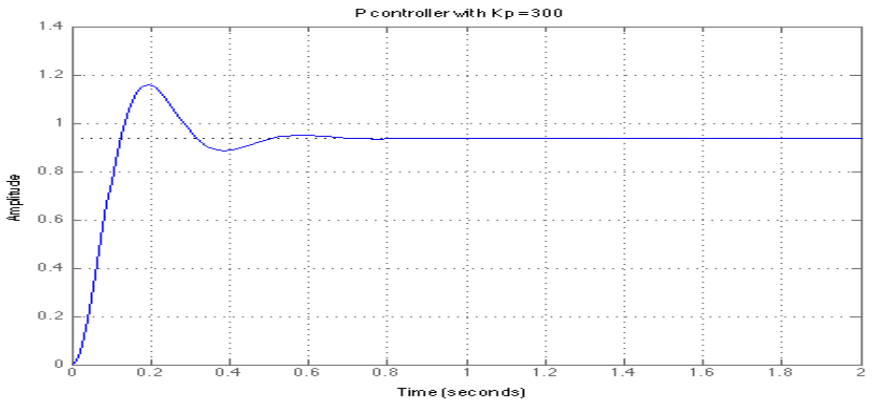

Figure 5.4 P Controller with Kp=300

Obviously, proportional controller decreases the rising time and steady state error. Now, we decrease the K_p from 300 to 100, we get the result as below:

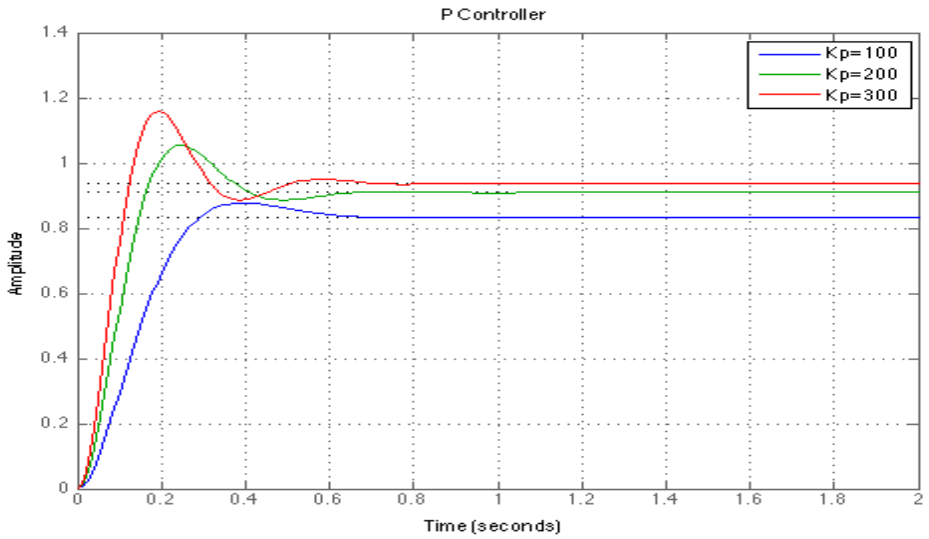

Figure 5.5 P Controllers with Kp = 100, 200, 300

This figure proves that larger K_p will decrease the rising time and steady state error, but increase the over shot.

If we use PI controller here, we have transfer function:

$$T(s) = \frac{K_p s + K_s}{s^2 + 15s + (20 + K_p s + K_i)} \qquad (5.8)$$

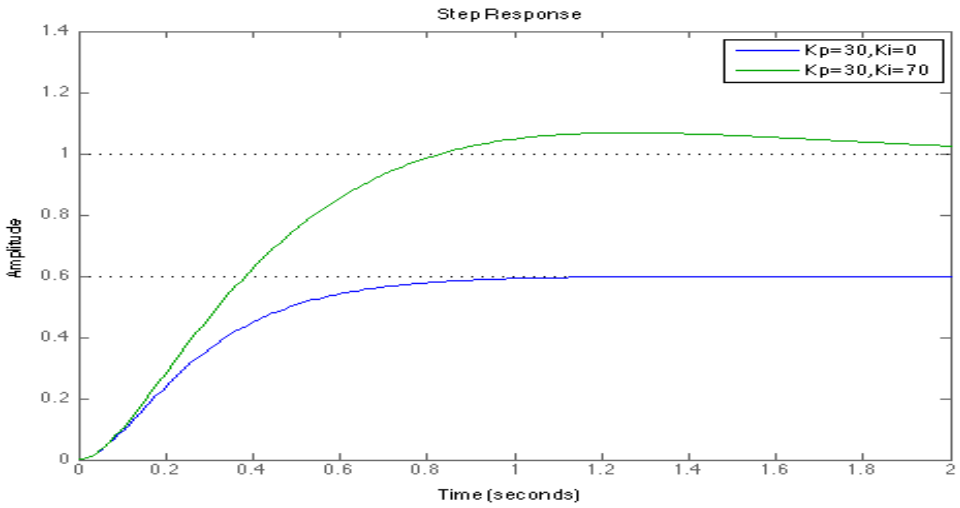

Figure 5.6 P-I Controllers with Kp=30, Ki =0 and Kp=30, Ki = 70

We have reduced the proportional gain (Kp) because the integral controller also reduces the rise time and increases the overshoot as the proportional controller does (double effect). The above response shows that the integral controller could eliminate the steady-state error.

Finally, we use the PID have discussed above. The transfer function becomes:

$$T(s) = \frac{K_d s^2 + K_p s + K_i}{s^2 + (10 + K_d)s + (20 + K_p)s + K_i} \qquad (5.9)$$

The step response is shown as below:

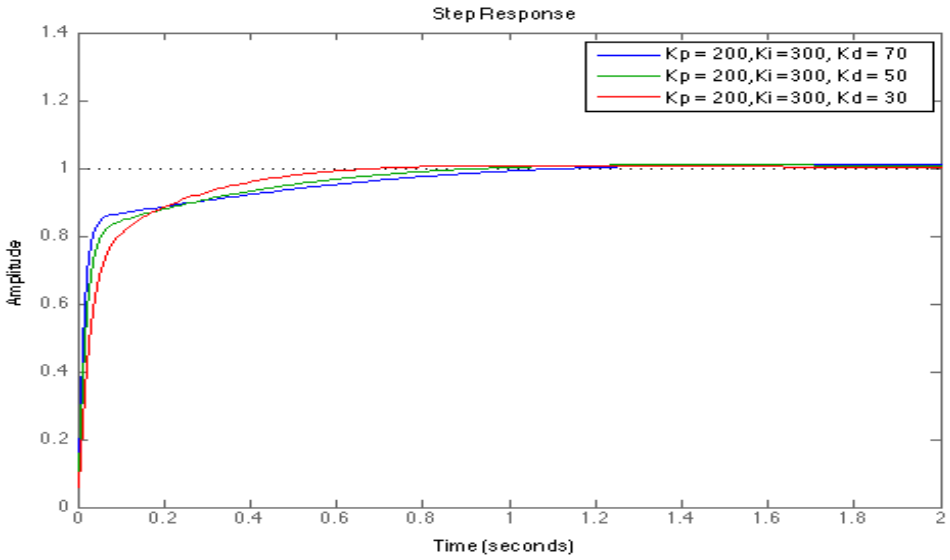

Figure 5.7 Step Response of Different PID controllers

Above figure demonstrates that larger K_d could decrease the rising time, but increase settling time and steady state error.

In sum, we could get table 5.1 below:

Table 5.1 The Relationship between PID Coefficients and Performance

Parameters	Rise time	Overshoot	Settling time	S-S Error
K_p	Decrease	Increase	Small Change	Decrease
K_d	Decrease	Increase	Increase	Eliminate
K_i	Small Change	Decrease	Decrease	No change

Chapter 6

Experiment Results

6.1 WGM Coupling Without PID

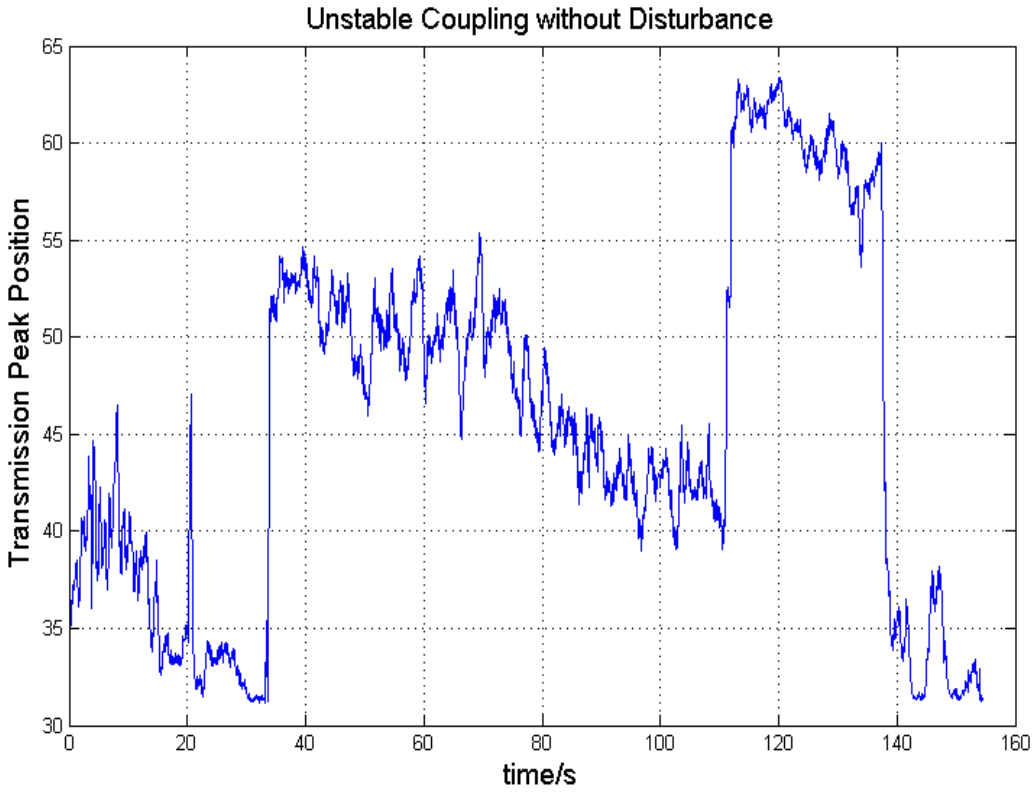

Figure 6.1 WGM Coupling Without Disturbance

Figure 6.1 display the coupling states in the long term in different coupling situations. We can see that even if there is no air flow from outside, the coupling is extremely unstable in the whole process. From 35 second to 110 second, due to unstable

mechanical control of Piezo controller stage, the transmission peak position downscaled from 53 to 40, which could introduce a negative effect to the coupling system and degrade other related experiments using WGM microresonator for sensing. At 110 second, we tuned the position of microresonators, but the transmission peak position still drop down in the next 30 second for the same mechanical issues.

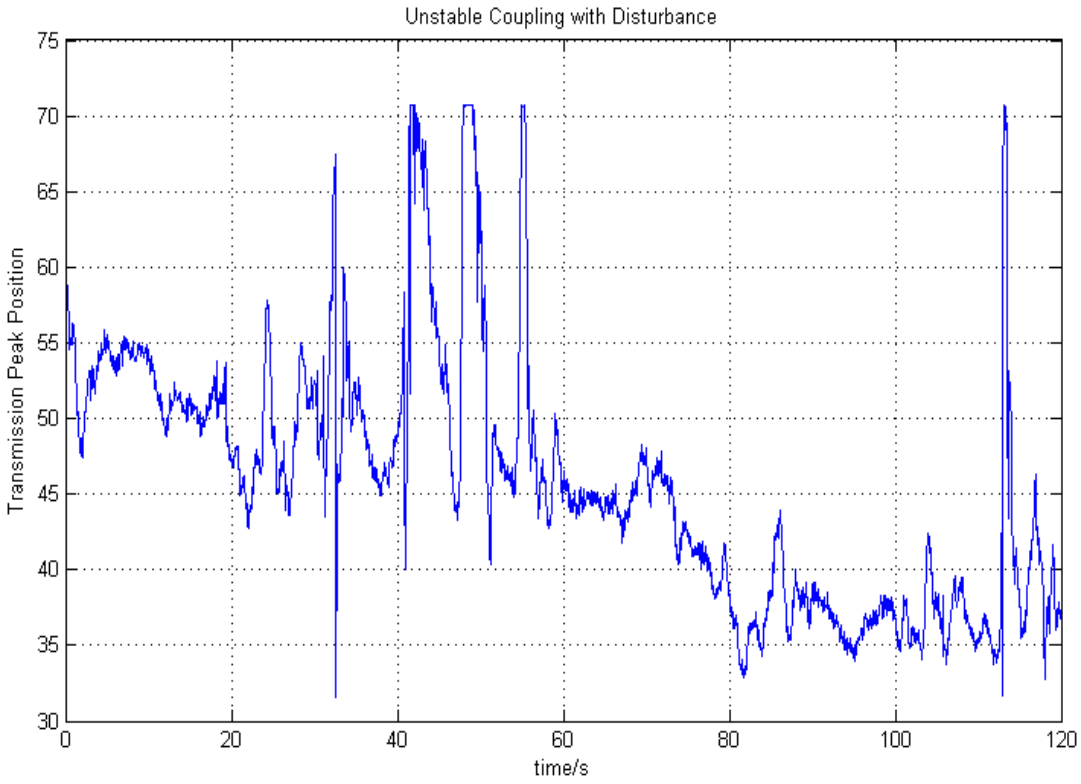

Figure6.2 WGM Coupling with Disturbance

Figure 6.2 display how the WGM coupling system responses to the air flow from surrounding environment. For the aim of simulation, I waved hand at 30 second. The position of peak fluctuates severely, which means coupling is deteriorated obviously. Without PID controller, the position of microtoroid cannot be pulled back.

6.2 Control Performance

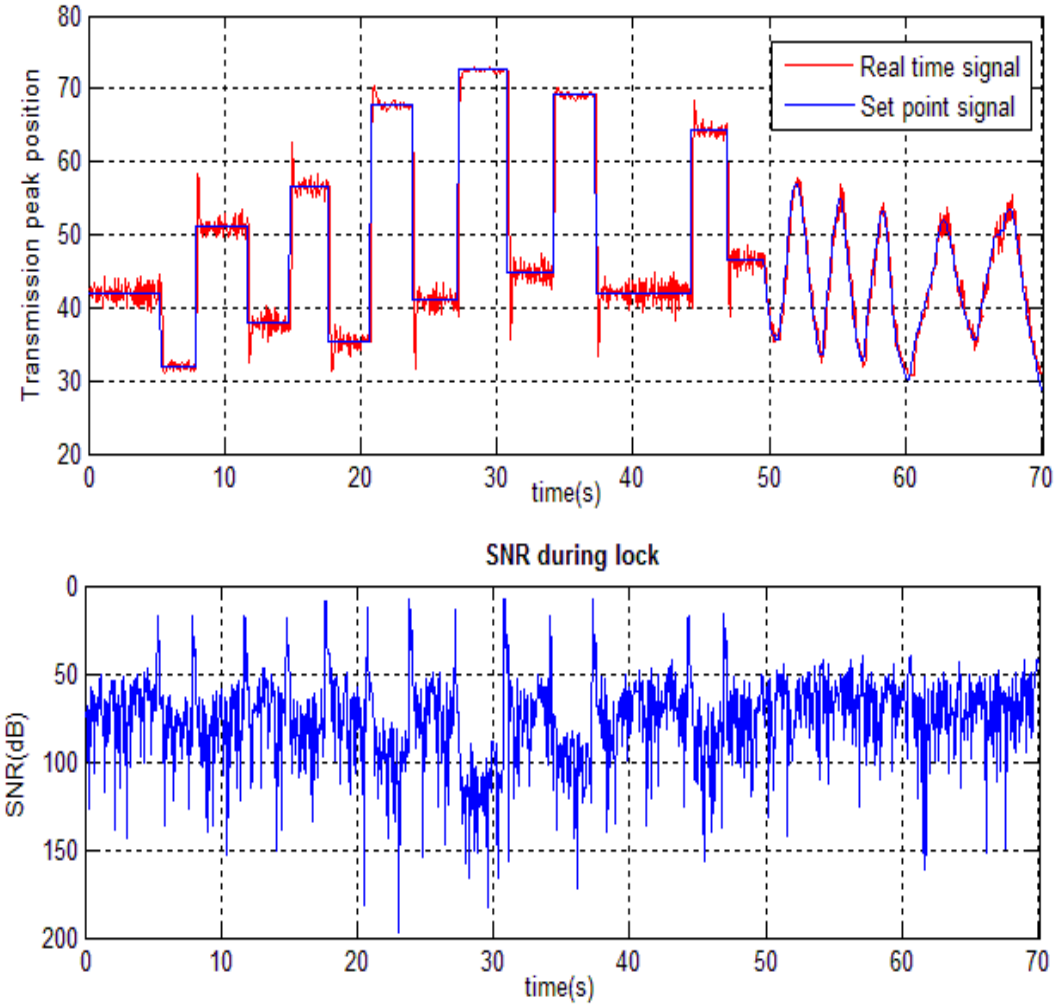

Figure 6.3 PID Controller Control Performances

Figure 6.3 shows the result of control process. We can see the performance of controller satisfies our requirement. The average SNR during the control is about 76 dB and the worst case is around 7dB. PID coefficient for the experiment is K_p=0.6, K_d=600, K_i= 60000. At 8, 12, 17, 22, 25, 27, 31, 34, 37, we tune the position suddenly, the step response shows the overshoot at some points, corresponding SNR are also worse than others. However, some points, like 27,31, there are almost none overshot. It is because system function is a complicate nonlinear system at different

coupling conditions, shown in Figure 6.4.

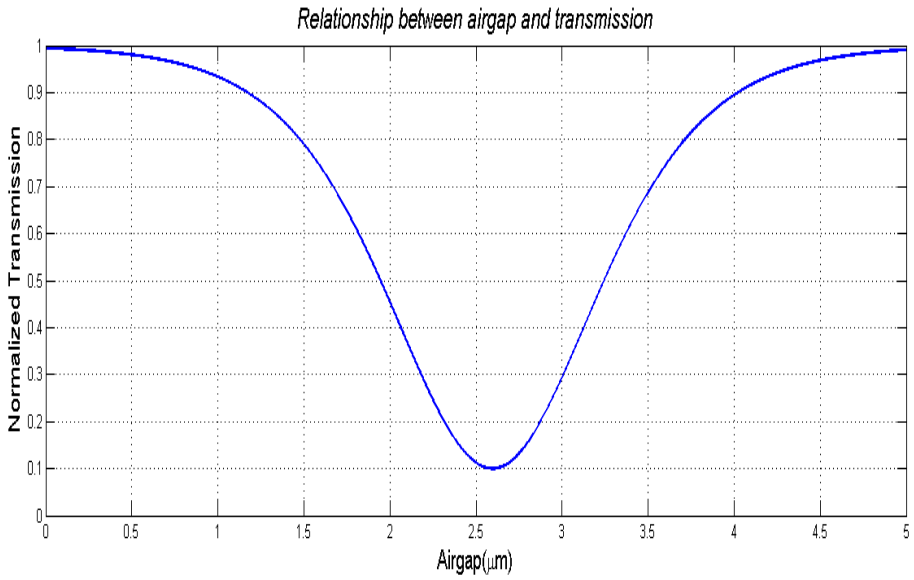

Figure6.4 Relationship between Airgap Distance and Normalized Transmission

Duet to this nonlinearity, we should change the PID coefficients to avoid overshoot. However, we could still regard it as a linear system at a specific range, which means the transmission is proportional to the air gap. Based on this assumption, the PID controller could still realize our design.

6.3 Stabilization Performance

In this section, we will discuss the performance of stabilization functionality. The goal of this project is to stabilize the air gap distance. A stabilized coupling is the prerequisite for all experiments using WGM microtoroid.

To simulate the disturbance from surrounding environment, I waived hand at second 50 and 102 to introduce the air flow to coupling system. We can see from Figure5.3

that the fluctuations right after the air flow. However, due to the PID controller, peak value is pulled back in 1-2 second. And the system is back to stable.

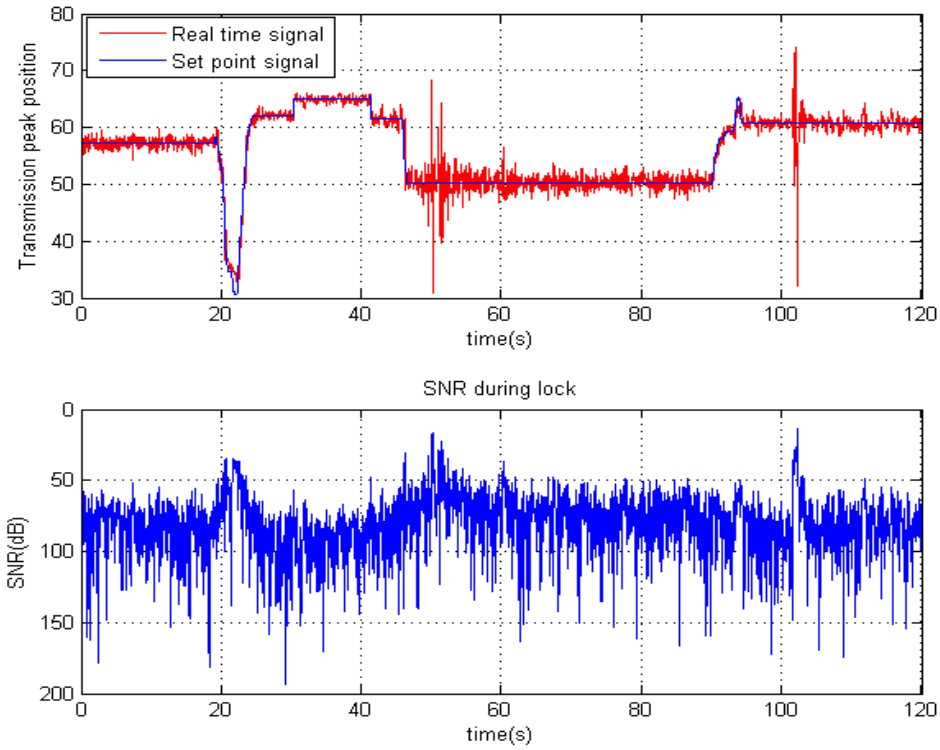

Figure6.5 Stabilization Experiments Result

6.4 Conclusions

This experiment proves that our PID controller could satisfy design requirement for coupling control and stabilization. Due to the nonlinearity of coupling, we cannot get accurate PID coefficients. By manually tuning, we obtain the approximately PID coefficients. With the help the PID controller, we could achieve a more stable research platform for many sensing experiments using WGM resonators.

References

[1] K.H. Ang, Chong, G.C.Y., and Li, Y. "PID control system analysis, design, and technology", *IEEE Trans Control Systems Tech*, 13(4), pp.559-576, 2005

[2] S. Arnold, D. Keng, S. I. Shopova, S. Holler, W. Zurawsky, and F. Vollmer, "Whispering gallery mode carousel C a photonic mechanism for enhanced nanoparticle detection in biosensing," *Opt. Express* 17, 6230-6238, 2009

[3] S. Bennett " A History of Control Engineering", *P. Peregrinus on behalf of the Institution of Electrical Engineers, London*, c1993

[4] Rick Bitter, " LabVIEW Advanced Programming Techniques", *CRC Press/Taylor & Francis Group*, c2007

[5] Ming Cai, Oskar Painter, and Kerry J. Vahala, "Observation of Critical Coupling in a Fiber Taper to a Silica-Microsphere Whispering-Gallery Mode System". *Physical Review Letter*, 85, 74-77, 2000

[6] T. J. Kippenberg, S. M. Spillane, D.K Armani, B. Min, L. Yang and K. J. Vahala, "Fabrication, Coupling and Nonlinear Optics of Ultra-High-Q Micro-Sphere and Chip Based Toroid Microcavitites" In K. J. Vahala, editor, *Optical Microcavities*, World Science, 2004

[7] Yang Lan, "Fabrication and Characterization of microlasers by the sol-gel method", PhD Thesis, California Institute of Technology, 2005

[8] Margolis Michael, " Arduino Cookbook", *O'Reilly*, c2012

[9] Bo Peng, Sahin Kaya Ozdemir, Jiangang Zhu, and Lan Yang, "Photonic molecules formed by coupled hybrid resonators", *Optics Letters*, Vol. 37, Issue**16**, pp. 3435-3437, 2012

[9] G. C. Righini, Y. Dumeige, P. Feron, M. Ferrari, G. N. Conti, D. Ristic and S. Soria, " Whispering Gallery Mode Microresonators: Fundamentals and Applications", *Rivista Del Nuovo Gimento*, Vol. 34, N. 7, 2011

[10] Jiangang Zhu, *Ultra-high-Q Microresonator with Applications towards Single Nanoparticle Sensing*. PhD dissertation, Washington University in Saint Louis, 2011.

[11] J. Zhu, et. al., "On-chip Single Particle Detection and Sizing by Mode Splitting in a Ultra-high-Q Microtoroid", Nature Photonics, 4, 46, 2010